CrossMark

Immobilization of Green Synthesized Silver Nanoparticles onto Amino-Functionalized Silica and Their Application for Indigo Carmine Dye Removal

Ali H. Gemeay · Eman F. Aboelfetoh (ORCID) ·
Rehab G. El-Sharkawy

Abstract In the present work, we have applied a green method for the synthesis of silver nanoparticles (AgNPs) onto amino-functionalized silica using *Nigella sativa* (black seed) aqueous extract as an eco-friendly and efficient reducing agent. The factors influencing the functionalization of silica and AgNPs loading have been considered. The samples were characterized by elemental analysis, FTIR, XRD, TGA, SEM, and EDX and used for the removal of indigo carmine (IC) dye from aqueous solution. The mean particle size of immobilized AgNPs was calculated from the XRD pattern using the Scherrer equation and is equal to about 26 nm. Adsorption experiments were carried out as batch studies at different contact times, temperature, adsorbent dosage, and initial dye concentrations. The IC adsorption equilibrium was attained after about 20 min of contact time. The equilibrium data shows that the Langmuir model was more reasonable to depict the IC adsorption, and the maximum adsorption capacity of IC is 73.05 mg/g. Based on the kinetic analysis, the adsorption process follows a pseudo-second-order equation. The estimation of the thermodynamic parameters such as the Gibbs free energy, entropy, and enthalpy changes of the adsorption process indicated the feasibility and endothermic nature of IC adsorption. The modified surface was found to be extremely stable in the aqueous medium, and no significant leaching of AgNPs was observed. Thus, immobilization of AgNPs may advance reuse, reduce environmental risks associated with leaching of AgNPs, and enhance cost-effectiveness.

Keywords Green synthesis · Silver nanoparticles · Silica · Adsorption · Isotherm · Kinetics

1 Introduction

In recent years, there has been impressive interest in silver nanoparticles (AgNPs) due to their wide-range applications in catalysis, sensors, antibacterial activity, and water purification (Aboelfetoh et al. 2017; Ghosh and Vandana 2017). Various methods have been applied to synthesize the silver nanoparticles, e.g., chemical reduction (Agnihotri et al. 2014), electrochemical techniques (Nasretdinova et al. 2015), photochemical reduction (Gabriel et al. 2017), and sonochemical (Elsupikhe et al. 2015), microwave-assisted (Ider et al. 2017), and radiation-assisted (Yue et al. 2017) processes. Although chemical reduction method is the most commonly used, it remains expensive or employs hazardous substances, such as organic solvents and toxic reducing agents, e.g., sodium borohydride, hydrazine, and N,N-dimethylformamide. Due to the high surface energy of the nanoparticles and forming aggregates, surface passivation and capping reagents are frequently added to the reaction systems (Vilchis-Nestor et al. 2014). The state-of-the-art studies have focused on the green synthesis approaches to avoid using hazardous materials. Plant-mediated syntheses of AgNPs have gained more

A. H. Gemeay · E. F. Aboelfetoh (✉) · R. G. El-Sharkawy
Chemistry Department, Faculty of Science, Tanta University, Tanta, Egypt
e-mail: eman.fahmy@science.tanta.edu.eg

Springer

importance than those prepared chemically due to the effectiveness of the process in terms of costs, time, ease of accessibility, etc. (Siddiqui et al. 2017; Sun et al. 2014). Among various plants, *Nigella sativa*, generally known as black seed, black cumin, or cumin noir, is commonly grown in the Middle East, Eastern Europe, and Western and Middle Asia (Randhawa et al. 2017). It has been traditionally used to treat various ailments and conditions that include hypertension, asthma, inflammation, diabetes, and bronchitis. Also, it has shown various activities such as antioxidant, antibacterial, and anticancer (Aljabre et al. 2015). The main active components separated from *Nigella sativa* seeds are alkaloids, thymoquinone, vitamins (as niacin, thiamin, riboflavin, pyridoxine, and folic acid), proteins, and minerals (Mosbah et al. 2017).

The residual dyes from different industrial sources are considered one of the most dangerous contaminants. In particular, the release of dye-containing effluents into the water environment is undesirable due to their color, as well as most dyes are toxic and carcinogenic or mutagenic to biota (Aboelfetoh et al. 2017; Zhang et al. 2016). Different methods were applied to remove dyes and various contaminants from water and wastewater (Aboubaraka et al. 2017; Gemeay et al. 2017; Habib et al. 2017; Khurana et al. 2017). Among them, the adsorption process by solid adsorbents demonstrates the possibility that it is one of the most efficient methods to eliminate various contaminants in wastewater treatment. This method depends on the transfer of pollutants from the solution to the solid phase. Moreover, adsorption is characterized by its simplicity operation, minimum sludge production, low cost, and relevance even at lower pollutant concentrations (Wu et al. 2016). Among inorganic compounds, silica has been used as a proficient material for the removal of pollutants because of its accessibility, low degree of swelling, stability, and controlled porosity. The chemical reactivity of its surface is a result of the presence of silanol groups (Jal et al. 2004; Zhu et al. 2017). Direct bonding of chelating groups to silica surface is troublesome because of relative inactivity of the surface in its ground state. However, this can be accomplished by surface activation/modification (Jal et al. 2004). Surface alteration via functional group immobilization provides unique opportunity to design the interfacial properties of solid substrates while retaining their mechanical strength and basic geometry. A new class of functionalized silica gel was synthesized by modifying it with different organic groups to tune

their characteristics for effective adsorption (Dolatyari et al. 2016).

The adsorption ability of the functionalized silica can be upgraded by loading it with AgNPs. Therefore, we have assessed the potential use of AgNPs loaded on functionalized silica, as a new and environmentally safe absorbent for the removal of indigo carmine (IC). This method includes the in situ reduction of aqueous silver ions employing *Nigella sativa* aqueous extract as a reducing agent in the presence of the amino-functionalized silica (f-silica). The composite materials (AgNPs/f-silica) exhibited very good performance for removing IC from aqueous solution. XRD, FTIR, SEM, TGA, and EDX techniques were used to describe the prepared materials, Moreover, the impacts of vital experimental factors (including black seed extract concentration, silver concentration, stirring time, pH, contact time, and adsorbent dosage, dye concentration, and temperature) were considered to get the optimum adsorption conditions.

2 Experimental

2.1 Materials and Methods

The standard solutions and dilution were made using double-distilled water following standard procedures. Silver nitrate (99%) was acquired from Sigma-Aldrich and used as received. 3-Aminopropyltrimethoxysilane (APTMS; 95%) and indigo carmine dye were obtained from Across, and silica gel (60–120 mesh) with particle size 0.063–2 mm was obtained from Baker (England). It has an estimated surface area of 200 m^2/g.

2.2 Synthesis of 3-Amino-Functionalized Silica

The coupling agent APTMS was used for the functionalization of the silica surface. The synthesis procedure was assembled from comparable studies with a few adjustments (Ncube et al. 2017; Yoncheva et al. 2014). Before functionalization, pretreatment of silica gel completed to dispose of the conceivable surface contaminants and activate the silanol groups on the surface. Activation was accomplished by treating 10.0 g silica gel with 200 mL of 0.02 M acetic acid for 2 h. Then, it had been filtered and washed several times with distilled water until pH 6 is obtained. Thereafter, it had been exchanged to a round-bottomed flask containing 50 mL toluene and 15 mL of APTMS. The mixture was stirred under reflux

(111 °C) for 3 h under inert atmosphere. The resulting product was filtered off, washed with ethanol, and dried at 55 °C for 24 h. Elemental analysis of the amino-functionalized silica (f-silica) was investigated to reveal the percentage of carbon, hydrogen, and nitrogen. The percentage was 4.15, 2.01, and 1.46% for C, H, and N, respectively, confirming the surface modification of silica with APTMS.

2.3 Preparation of *Nigella sativa* Aqueous Extract

Nigella sativa seeds, Egyptian ranches, were washed a few times with refined water. Twenty grams of coarsely ground seeds was boiled in 100 mL of twofold distilled water for 15 min and sifted through Whitman No. 1 filter paper. The filtrate was gathered and put away at 4 °C for further utilization.

2.4 Synthesis of Immobilized Silver Nanoparticles

AgNPs immobilized on functionalized silica gel have been synthesized via in situ green reduction of Ag^+ by adding a certain volume of *Nigella sativa* aqueous extract. A typical reaction mixture contains 2 g of functionalized silica gel soaked in 50 mL distilled water with stirring for 30 min, accompanied by adding $AgNO_3$ solution and a certain volume of aqueous extract, and the total volume was adjusted to 100 mL. To optimize the formation of AgNPs, the concentration of $AgNO_3$ was varied within the range 0.005–0.07 mol/L, while the extract concentrations were varied in the range 2–10% (*v/v*). For reactions, the mixture was refluxed at 100 °C for 30 min. The formation of immobilized AgNPs was observed via changing the color of the functionalized silica particles from yellow to brownish and, finally, to deep brown. The particles were filtered, washed several times using distilled water, and finally dried at 60 °C overnight. The formation of AgNPs was confirmed by mixing the $AgNO_3$ solution and extract solution in the absence of modified silica particles. The reduction of silver ions to AgNPs was tested by a UV–vis spectrophotometer (Fig. 1). The colorless $AgNO_3$ solution turning out to be dark brownish yellow color indicated the formation of AgNPs. The intense band detected around 420 nm was defined as a *surface plasmon resonance band* and ascribed to the excitation of free electrons in AgNPs (Aboelfetoh et al. 2017).

Morphology of Ag-NPs/f-silica was examined by SEM (JEOL JSM-6510 TV). EDX (Rontec, M-series,

EDR288/SPU2) analysis was used to study the surface distribution of silver within all synthesized samples. The XRD measurements were done by MXP-18 (Mac Science Co., Ltd) with monochromatic CuKα radiation. Infrared spectra were recorded on an FTIR spectrophotometer (PerkinElmer 1430) to identify the chemical structure of the samples. The KBr disc technique was used to prepare FTIR samples. Thermal gravimetric analysis (TGA) measurements were done using the Shimadzu TGA-50 thermogravimetric analyzer (Shimadzu, Japan) over the temperature range 25–1000 °C at the heating rate 15 °C/min in the N_2 atmosphere. Elemental analysis (CHNS) was determined using the PerkinElmer CHNS/O analyzer. The concentrations of the IC were measured using a spectrophotometric strategy. Calibration curve of the dye was set up by measuring their absorbance against concentration at $\lambda_{max} = 610$ nm using the Shimadzu 2100S UV–vis spectrophotometer (Japan) with 1.0-cm-path length cell.

# 3 Results and Discussion

3.1 Characterization

3.1.1 FTIR Measurements

The most important differences between the functionalized silica surface (f-silica) and the immobilized AgNPs onto functionalized silica surface (AgNPs/f-silica) are shown in Fig. 2(a, b). A broad absorption band at 3439 cm^{-1} was observed which assigned to silanol (Si–OH) groups on the surface. The strong bands at 462 and 1090–1100 cm^{-1} indicate the bending and asymmetric stretching of siloxane (Si–O–Si) groups. The band at 2929 cm^{-1} was ascribed to symmetric vibration of the C–H groups. Absorption bands at 3456 and 1571 cm^{-1} represent the stretching and bending vibration of aliphatic amine (N–H) groups (Banaei et al. 2017). FTIR assessment was also carried out to identify the potential biomolecules in *Nigella sativa* aqueous extract responsible for the synthesis of AgNPs. Previously, it was reported that *Nigella sativa* seeds contain various alkaloids, amino acid, saponins, flavonoids, steroids, protein, and terpenoids (Nivetha and Prasanna 2016).

The spectrum of *Nigella sativa* extract (Fig. 2(c)) showed a number of bands, thus reflecting a complex nature of the aqueous extract. The band at 3428 cm^{-1}

Scheme 1 Synthetic procedure for AgNPs/f-silica composite and a proposed mechanism for adsorption of IC dye
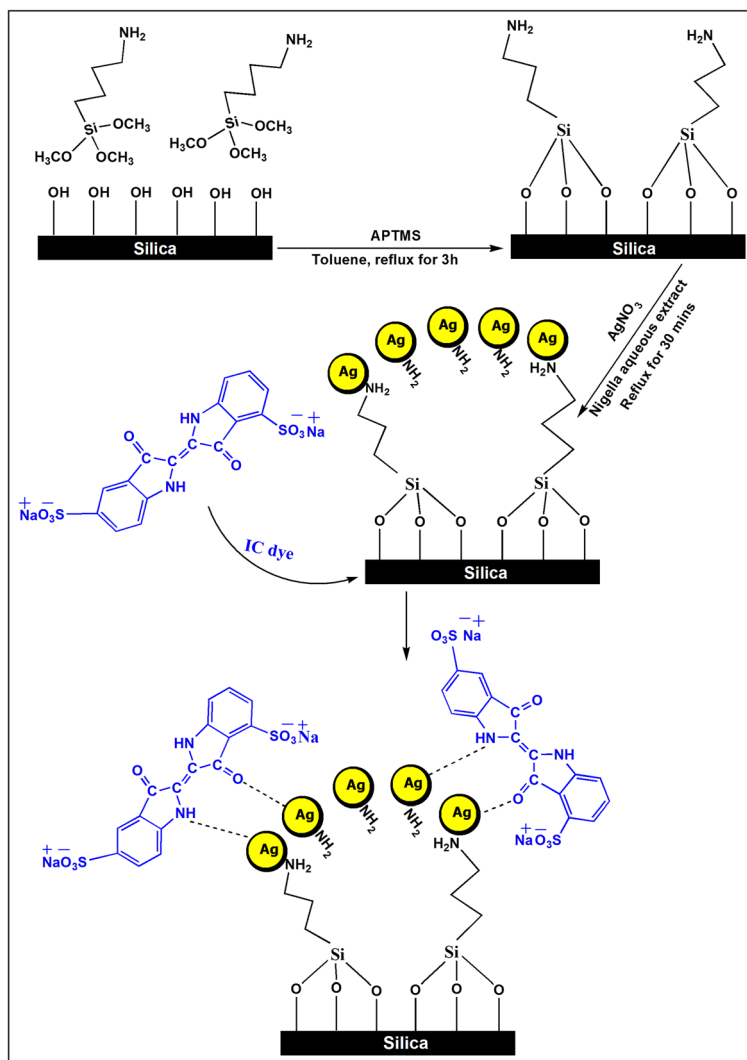

could be related to the stretching vibration of amide (NH–), and the small bands at 2929 and 2859 cm^{-1} were ascribed to the symmetric vibration of the C–H groups. A sharp intense band at 1613 cm^{-1} can be due to the stretching vibration of aromatic C=C or C–N bending in the amide group (Amooaghaie et al. 2015). The main bands existing in the aqueous extract are also present in the FTIR spectrum of the synthesized AgNPs onto functionalized silica (AgNPs/f-silica) with lower intensities and small shift (Fig. 2(b)). This strongly suggests the synergistic effect of all the constituents present in *Nigella sativa* aqueous extract that act not only as excellent reducing agents to reduce the Ag ions to the corresponding AgNPs but also as stabilizers of the synthesized AgNPs.

3.1.2 X-Ray Diffraction

The XRD patterns for silica, amino-functionalized silica (f-silica), and AgNPs loaded onto functionalized silica (AgNPs/f-silica) (Fig. 3a) were characterized by a broad peak at around $2\theta = 22.3°$, reflecting the partially amorphous nature of silica matrix (Aboelfetoh and Pietschnig 2009). Additionally, the AgNPs/f-silica (S1) showed small broad peaks at 2θ values of 38.13°, 44.25°, 64.78°, and 77.60°. The sets of corresponding lattice planes were observed, which may be well indexed to the (111), (200), (220), and (311) facts of AgNPs. Moreover, it is evident that for silica-loaded AgNPs composite (S4), diffraction peaks become more intense and narrow with the increasing concentration of silver,

Fig. 1 UV-visible spectra of
Nigella sativa (black seed)
aqueous extract and AgNPs
colloidal solution obtained by
reduction with the extract at
100 °C for 30 min
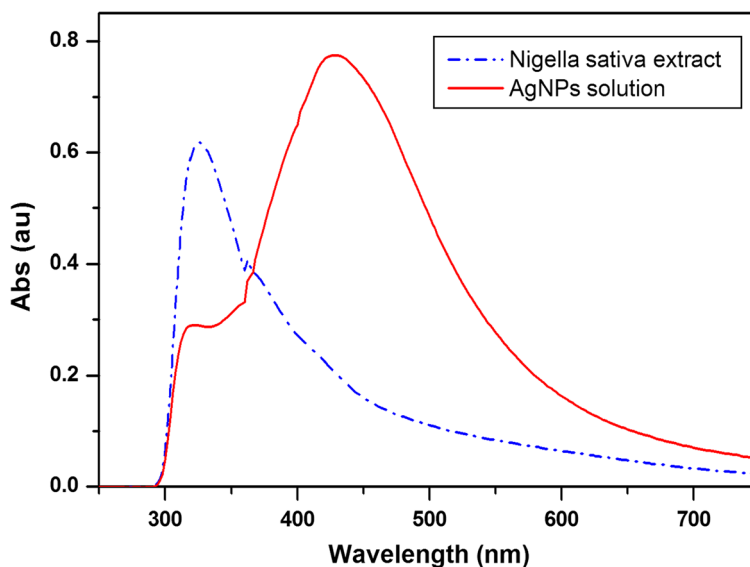
suggesting that the average particle size also increases.
The XRD patterns thus clearly show that the AgNPs
formed by the reduction of Ag^+ ions by *Nigella sativa*
aqueous extract is crystalline in nature similar to earlier
published results (Dhanalekshmi and Meena 2014). The
average grain size of the AgNPs was determined using
the Scherrer equation (around 26 nm).

3.1.3 TGA Analysis

Thermogravimetric analysis was recorded under N_2
atmosphere over the temperature range of 25–

800 °C at a heating rate of 15 °C/min to evaluate
both the composition and the thermal stability of f-
silica and AgNPs/f-silica. As proven in Fig. 3b, the
mass loss noticed between 25 and 180 °C represents
the physically adsorbed water. Adsorbed water
accounted 7.4, 6.43, and 2.2% for f-silica, AgNPs/
f-silica sample using $[Ag^+] = 0.005$ M, and AgNPs/f-
silica sample using $[Ag^+] = 0.05$ M, respectively.
The decrease in the amount of physically adsorbed
water can be attributed to the increasing amount of
AgNPs anchoring on the functionalized silica sur-
face, which is due to the increase of the precursor

Fig. 2 FTIR spectra of amino-
functionalized silica (f-silica) (a),
AgNPs/f-silica (b), and the aque-
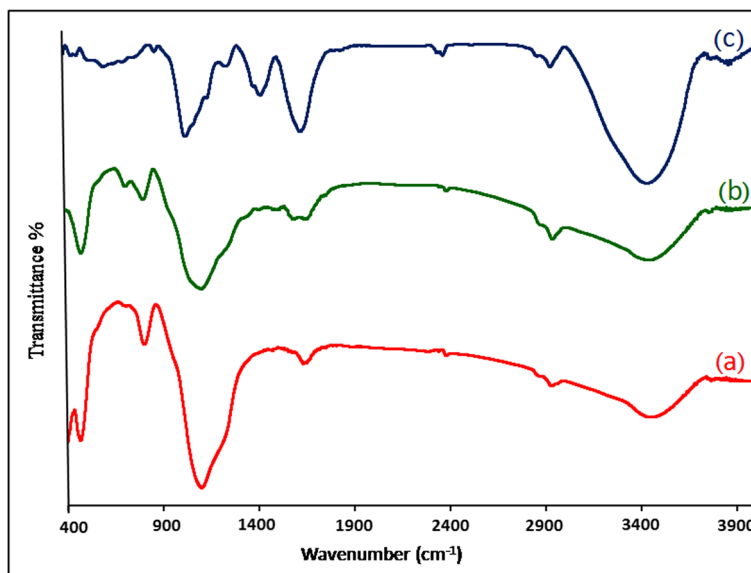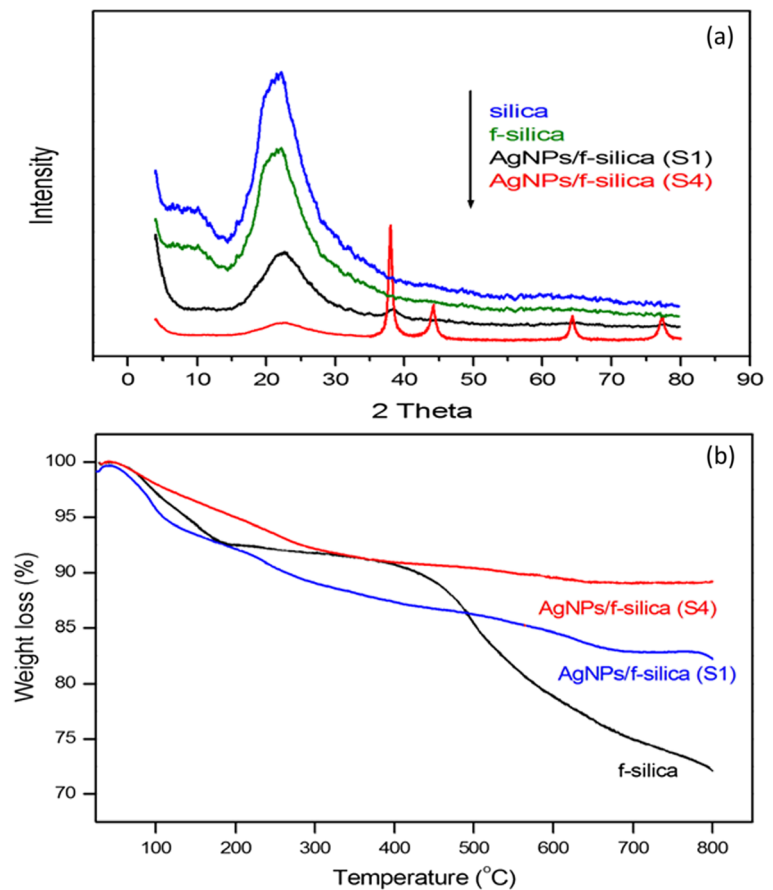ous extract of *Nigella sativa* (c)

Fig. 3 XRD patterns of silica, amino-functionalized silica (f-silica), and AgNPs/f-silica samples (**a**) and TGA analysis of amino-functionalized silica (f-silica) and AgNPs/f-silica (S1 and S4 samples) (**b**)

[Ag$^+$]. The second weight loss commenced from 387 to 545 °C is observed for the f-silica sample with a value of 9.51% and is associated with the decomposition of the aminopropyl groups within the sample. This stepwise decomposition performance of the aminopropyl group is reliable with the earlier reports (Khdary et al. 2014; Zhang et al. 2008). Weight loss above 550 °C was observed for all three samples with the values of 47, 66.3, and 3.2%, respectively, which is likely due to the further condensation of SiOH groups (Khdary et al. 2014) which is additional evidence for the attachment of the linker to the silica. It can be concluded that the maximum decomposition temperature was lowered slightly after AgNPs deposition on f-silica, but the overall thermal stability was extremely increased. The same behavior was observed for the samples prepared with increasing the stirring time. An increased of stirring time helped in forming more AgNPs onto the f-silica and increased thermal stability. This demonstrates that the aminopropyl groups could give

binding sites for the adsorption of silver ions on the silica. The silver ions with empty orbital were thought to be immediately adsorbed, thus encompassing the amino groups through electrostatic interaction due to the lone pair of electrons that exist on the nitrogen atoms of the amino groups (Dong et al. 2014). The addition of *Nigella sativa* extract led to the reduction of Ag$^+$ ions and subsequent formation of AgNPs.

3.1.4 SEM and EDX Analysis

The surface morphology of AgNPs anchoring on functionalized silica (AgNPs/f-silica) was evaluated utilizing SEM. The micrograph revealed that the AgNPs are well dispersed on the surface, exhibiting mainly spherical shape at the nanoscale (Fig. 4a). Moreover, the EDX analysis for AgNPs/f-silica confirms the presence and homogeneous distribution of Ag on the silica surface (Fig. 4b).

4 Batch Adsorption Studies

In this work, IC dye was picked as a model to study the sorption activity of AgNPs/f-silica. The stock solution of IC (10^{-4} M) was prepared in 1000 mL of distilled water in a measuring flask. Twenty-five milliliters of the dye solution was mixed with 10 mg of functionalized silica (f-silica) at 30 °C, and the mixture was put into a 100-mL conical flask and agitated for 3 h to observe the adsorption situation of the unmodified surface. The solution was centrifuged, the absorbance was monitored spectrophotometrically, and a slight decrease (20%) in the absorbance was observed. Thus, to evaluate the adsorption properties of modified silica surface with AgNPs, a series of adsorption experiments was conducted. Typically, 25 mL of IC solution was added into a set of 100-mL stoppered flasks that contained 10 mg solid adsorbent. The flasks were kept in a shaker thermostat at a speed of 120 rpm. After predetermined time intervals, the sample solutions were filtered to determine the residual concentrations. The IC concentrations in the initial and final aqueous solutions were measured by using a UV–vis spectrophotometer at 610 nm (Fig. 5). The equilibrium adsorption capacities (q_e) were calculated according to the following formula (Eq. 1):

$$q_e = (c_0 - c_e)\frac{V}{m} \qquad (1)$$
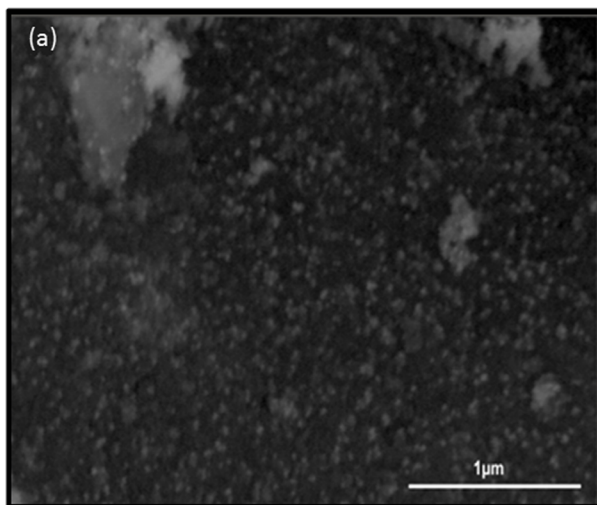
The dye removal (%) was determined by the following equation (Eq. 2):

$$Removal\ (\%) = \left[\frac{(c_0 - c_e)}{c_e}\right] \times 100 \qquad (2)$$

where c_0 (mg/L) and c_e (mg/L) indicate the initial and equilibrium concentrations of IC in solution, respectively. The impacts of IC concentration, contact time, pH, and temperature on adsorption were examined. The adsorption kinetics was studied by analyzing adsorption capacity of the aqueous solution at assorted time intervals.

4.1 Variation of AgNPs/Functionalized Silica Composition

The proficiency of AgNPs/f-silica samples for the adsorptive elimination of IC from aqueous solutions has been assessed with respect to several synthesis factors to obtain composites having high adsorption activity. These factors are [Ag], [*Nigella* seed], and the reflux time. The synthesis conditions, the abbreviation symbol, and the IC removal efficiency of each sample are listed in Table 1.

4.1.1 Effect of [Ag]

The effect of AgNPs/f-silica samples prepared at different AgNO$_3$ concentrations on the adsorption rate of the
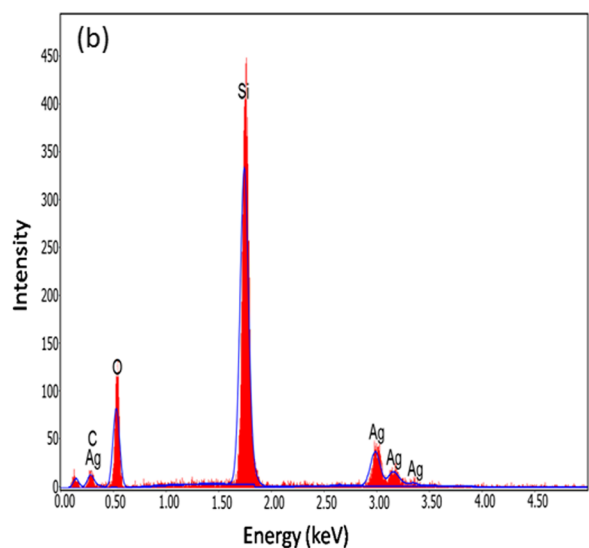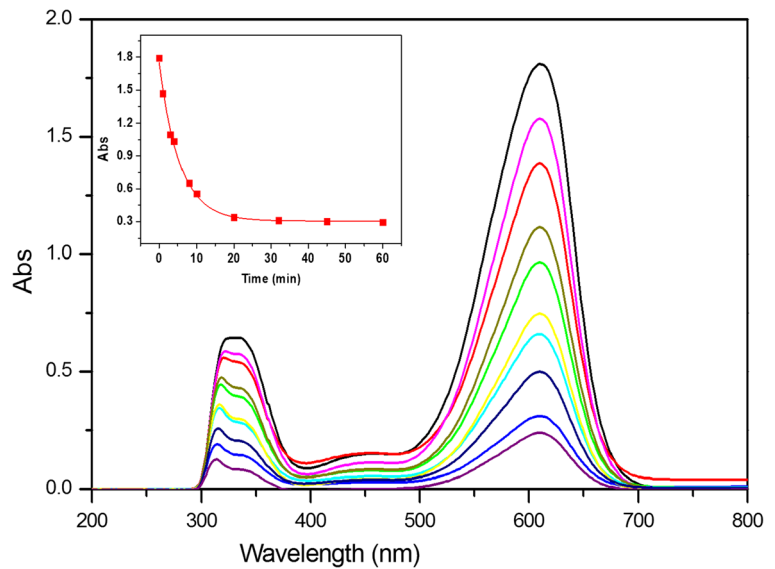

Fig. 4 SEM image (**a**) and EDX spectrum (**b**) of AgNPs/f-silica

Fig. 5 UV-vis spectra of IC (55.69 mg/L) at various time intervals in presence of AgNPs/f-silica sample (S1)

IC was tested (Fig. 6a, Table 1). The adsorption proficiency achieved a maximum at ca. 0.03 M (sample S3), and after that, it diminishes. This was likely because of the increase in the formation of larger particles of AgNPs as the [Ag] increased (Sinha et al. 2015; Venkatesham et al. 2014). Our findings seem to be well supported by the increase in the [Ag], prompting an increase in the density of nuclei that may lead to high collisions between nuclei. Thus, the production rate of AgNPs is improved, and therefore, an increase of particle size is acquired. It is sensible to express that the binding of the dye molecules to the AgNPs/f-silica relies upon the surface area accessible for interaction. Smaller particles having the larger surface area will give more adsorption efficiency than the larger particles and clusters.

4.1.2 Effect of [Nigella sativa Seed]

The effect of AgNPs/f-silica (S6–S9) samples prepared at various [Nigella seed] on the removal rate of the IC was studied (Fig. 6b). Values of q_e were calculated and listed (Table 1). It seems plausible that the Nigella sativa seed extract was able to kinetically control not only the growth rate of AgNPs but also the removal rate of IC. An increase of Nigella extract concentration, a greater amount of Ag$^+$ reduction, and large-sized clusters with broad size distribution were obtained (Sinha

et al. 2015). Again, AgNPs clusters have smaller surface areas for adsorption.

4.1.3 Effect of Stirring Time

The stirring time of Nigella seed extract for Ag$^+$ reduction was found to be an important factor to obtain AgNPs. The longer the stirring time, the more complete the attained reduction. Table 1 illustrates that the removal efficiency of IC increases with samples synthesized at a longer stirring time. This may be attributed to the increase in the yield of AgNPs.

4.2 Effect of Kinetic Variables

4.2.1 Effect of Contact Time and Initial IC Concentration

The adsorption of IC at various initial dye concentrations onto AgNPs/f-silica (S1) was investigated as a function of time to conclude the equilibrium time for maximum adsorption. It is apparent from Fig. 7a that the adsorption rate was rapid during the preliminary contact time (within the first 15 min) which can be attributed to the accessibility of the active sites of adsorbent. Therefore, an increase in the concentration of IC in solution and thus on AgNPs/f-silica (concentration gradient) tends to increase the dye adsorption rate at the initial stages. As time continues, this concentration gradient

Table 1 Preparation conditions of the synthesized AgNPs/f-silica samples and their IC removal efficiencies

Preparation conditions	The varied parameter	Sample symbol	q_e (mg/g)	Removal %
	[Ag] (M)			
[Black seed] = 5%	0.005	S1	50.80	82.60
Wt. of silica = 2.0 g	0.01	S2	52.95	85.46
Temp. = 100 °C	0.03	S3	57.93	90.34
Reflux time = 30 min	0.05	S4	51.19	86.98
	0.07	S5	46.50	80.53
	[black seed] (%)			
[Ag] = 0.01 M	2.0	S6	59.93	96.60
Wt. of silica = 2.0 g	5.0	S7	51.65	84.46
Temp. = 100 °C	7.0	S8	47.97	78.51
Reflux time = 30 min	10.0	S9	42.82	72.67
	Reflux time (h)			
[Ag] = 0.005 M	0.5	S10	49.96	80.60
[Black seed] = 5%	4.0	S11	51.93	85.63
Wt. of silica = 2.0 g	8.0	S12	64.90	92.75
Temp. = 100 °C				

diminishes due to the increased occupation of vacant sites by IC molecules. Thereafter, the adsorption rate increased gradually with equilibrium essentially being reached by 60 min (optimum contact time). The adsorption curves were single, smooth, and continuous up to the saturation state, demonstrating the conceivable formation of monolayer coverage on the adsorbent surface by the dye molecules (Elmorsi 2015).

4.2.2 Effect of Adsorbent Dosage

The adsorbent dosage decides the capacity of the adsorbent for a given initial concentration of dye solution. The removal percentage increased rapidly from 44.6 to 95.6% with the increase in the adsorbent dosage from 0.005 to 0.02 g. This might be ascribed to the accessibility of more active adsorption sites on the AgNPs/f-silica surface with increasing the dosage of the adsorbent.

4.2.3 Effect of pH

The solution pH has a great effect on the whole adsorption process, where it specifically affects the nature of the functional groups of both adsorbents and dye molecules. Subsequently, the influence of initial pH of IC solution on its removal by AgNPs/f-silica was examined. The pH adjustment was

done by phosphate-buffered solutions (0.067 M). The higher and lower pH values were obtained by adding a few drops of 0.1 M NaOH or 0.1 M HCl. The highest IC removal was observed at pH 2 (96.38%). As illustrated in Fig. 7b, the value of IC removal percentage decreased with increasing the pH from 2 to 12.

The variation in the dye uptake with respect to the initial solution pH can be explained in terms of the point of zero charge (PZC) of adsorbent as well as dye structure and its pK_a value. The pK_a value of IC is equal to 12.3, while the PZC of commercial AgNPs is equal to 3.5 (Liu et al. 2009). At pH < pH_{PZC}, the surfaces of the adsorbents are net positively charged, while at pH > pH_{PZC}, the surface charge of adsorbents is negatively charged. At a pH below pH_{PZC} (3.5), the surface of the adsorbent is positively charged, i.e., increase in the number of positively charged sorbent sites which leads to increasing the electrostatic attraction between anionic dye (IC) and adsorbent sites. At a pH above 3.5, the adsorbent sites become negative and thus repulsive interactions between IC and adsorbent sites lead to a reduction in adsorption capacity. In a basic medium, IC exhibits intra-molecular hydrogen bonding between the C=O and N–H within the molecule (Ansari and Mosayebzadeh 2011). This results in the weak intermolecular interactions of the IC molecule to AgNPs/f-silica.

Fig. 6 Removal percentage of IC (55.69 mg/L) by various AgNPs/f-silica samples prepared at **a** various [Ag] and **b** various [*Nigella* seed]
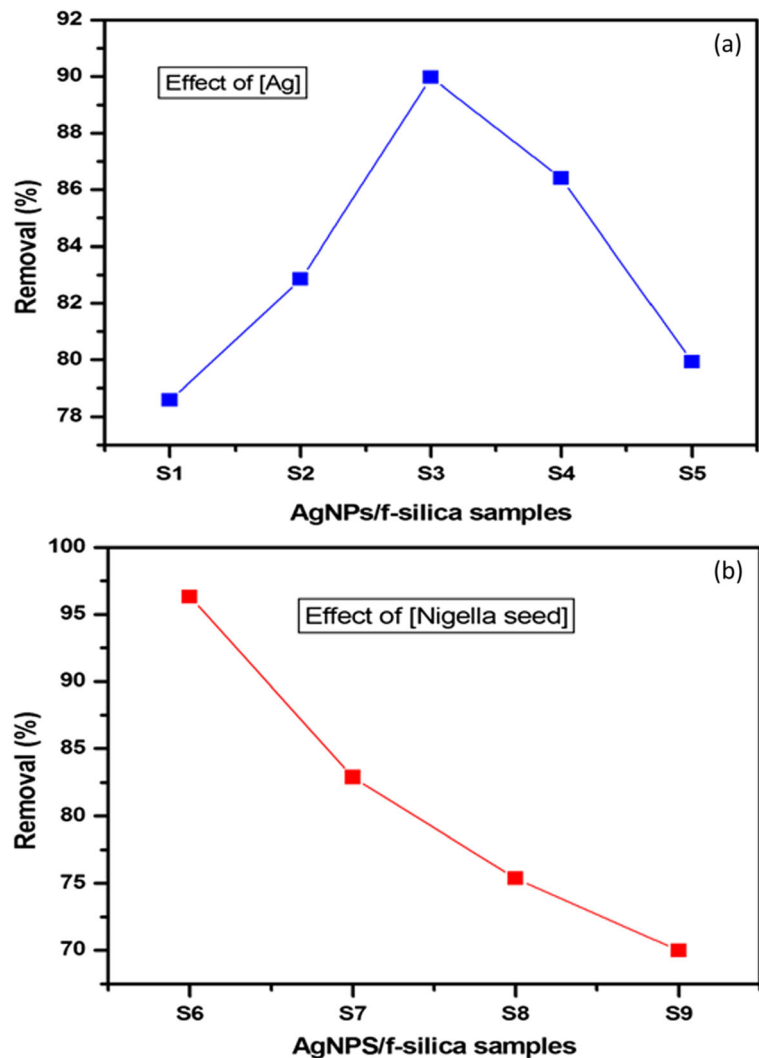
4.3 Adsorption Kinetic Study

Three well-known models were used to interpret the kinetics of adsorption process from aqueous solutions such as Lagergren pseudo-first-order, pseudo-second-order, and intra-particle diffusion equations. The linearized form of the first two models, Eqs. 3 and 4, is expressed as follows:

$$\log(q_e - q_t) = \log(q_e) - k_1/2.303\ t \qquad (3)$$

$$t/q_t = 1/k_2 q_e^2 + t/q_e \qquad (4)$$

where q_e (mg/g) and q_t (mg/g) are the adsorption capacity at equilibrium and at time t, respectively, and k_1 (min^{-1}) signifies the rate constant of the pseudo-first-order model. k_2 (gmg^{-1}min^{-1}) symbolizes the rate constant of the pseudo-second-order model. Values of k_1, k_2, and the corresponding correlation coefficient (R^2) were ascertained and depicted in Table 2. The theoretical values of q_e calculated from the pseudo-first-order model gave clearly dissimilar values compared with the experimental ones, which have slightly lower correlation coefficients. Therefore, this model appears to be unsuitable for the current AgNPs/f-silica/dye system. The R^2 values for the pseudo-second-order kinetic model were found to be higher, and the calculated q_e values were mostly close to the experimental data. This indicates that this model efficiently fits the adsorption data.

Fig. 7 Adsorption capacity of AgNPs/f-silica (0.01 g) at different time intervals with different initial IC concentrations (**a**) and removal percentage of IC (55.69 mg/L) by the AgNPs/f-silica sample (S1) at different pH values (**b**)
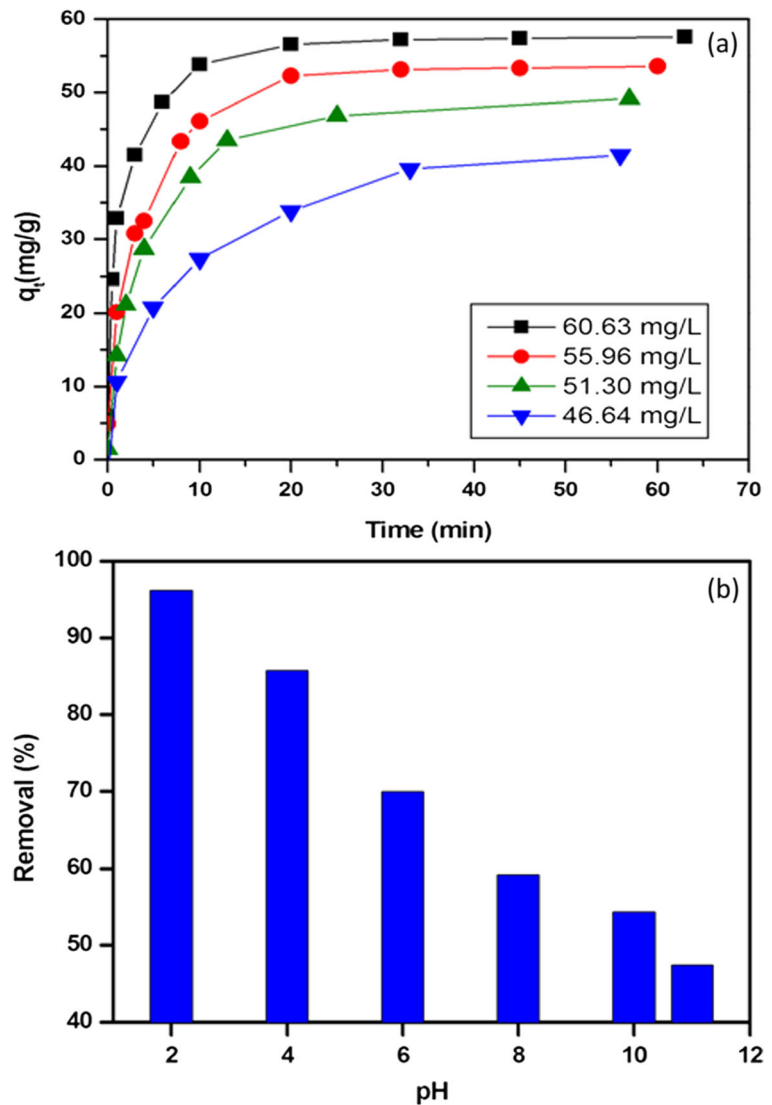
In general, the dye sorption is governed by the liquid-phase mass transport rate or the intra-particle mass transport rate. The dye species are most likely transported from the bulk of the solution into the solid phase with an intra-particle diffusion process, which is frequently the rate-limiting step in various adsorption processes. The possibility of intra-particle diffusion was examined by using the intra-particle diffusion model (Üner et al. 2016). The intra-particle diffusion model was expressed as follows (Eq. 5):

$$q_t = k_p t^{0.5} + C \qquad (5)$$

where q_t (mg/g) is the fraction dye uptake at time t, k_p (mgg^{-1}min$^{-0.5}$) is the intra-particle diffusion rate constant, and C (mg/g) is the intercept.

The values of C give a thought regarding the thickness of the boundary layer; i.e., the larger the intercept, the more prominent the contribution of the surface sorption in the rate-controlling step.

The plot gave two linear portions, suggesting that the IC adsorption comprises more than one kinetic step (Fig. 8). In the primary step, the dye is transported from solution through the particle–solution interface (external diffusion) and portrayed by k_{p1}. The second linear part is ascribed to the internal diffusion of IC molecules within the pores

Table 2 Parameters of pseudo-first-order, pseudo-second-order, and intra-particle diffusion models at different initial IC concentrations using the AgNPs/f-silica sample (S1)

| $[IC]_0$ (mg/L)	Pseudo-first-order model			Pseudo-second-order model				Intra-particle diffusion model					
	$q_{e, cal}$ (mg/g)	K_1 (min^{-1})	R^2	$q_{e, exp}$ (mg/g)	$q_{e, cal}$ (mg/g)	K_2 (gmg^{-1}min^{-1})	R^2	K_{p1} (mgg^{-1}min$^{-0.5}$)	C_1 (mg/g)	R_1^2	K_{p2} (mgg^{-1}min$^{-0.5}$)	C_2 (mg/g)	R_2^2
60.63	25.32	0.140	0.981	55.36	54.65	0.013	0.999	09.02	15.74	0.9858	0.45	45.98	0.8229
55.96	30.31	0.121	0.979	50.80	49.55	0.043	0.998	09.74	08.96	0.9980	0.67	42.70	0.8912
51.30	34.83	0.190	0.992	47.78	48.10	0.038	0.998	10.41	02.45	0.9931	0.99	38.64	0.8129
46.64	37.36	0.076	0.991	44.59	43.80	0.021	0.990	07.16	01.10	0.9976	0.94	32.07	0.9510

of the composite particles (intra-particle diffusion), which is characterized by k_{p2}. At this step, the diffusion resistance increases and causes the diffusion rate to diminish. With the continued uptake of the dye from the solution, the adsorption decreases until the final equilibrium is attained (Bhalara et al. 2015). In general, the adsorption process is controlled by this model if the plot of q_t vs. $t^{0.5}$ gives a straight line and passes through the origin. Here, the straight lines did not pass through the origin. This would appear to indicate that the intra-particle diffusion was involved in the adsorption process but was not the rate-limiting step. Therefore, the adsorption process of IC on the

synthesized composites could be due to the combined effect of external film diffusion and intra-particle diffusion (Yuan et al. 2017).

4.4 Thermodynamic Parameters

The effect of temperature on adsorption denotes knowledge into the adsorption behavior and mechanism. The heat change and spontaneity for the adsorption process might be revealed through the thermodynamic parameters such as the free energy of adsorption ($\Delta G°$), the enthalpy change ($\Delta H°$), and entropy change ($\Delta S°$). Both of $\Delta H°$ and $\Delta S°$ were assessed from the straight plot acquired

Fig. 8 Intra-particle diffusion plot of IC adsorption on the AgNPs/f-silica sample (S1) at different initial concentrations
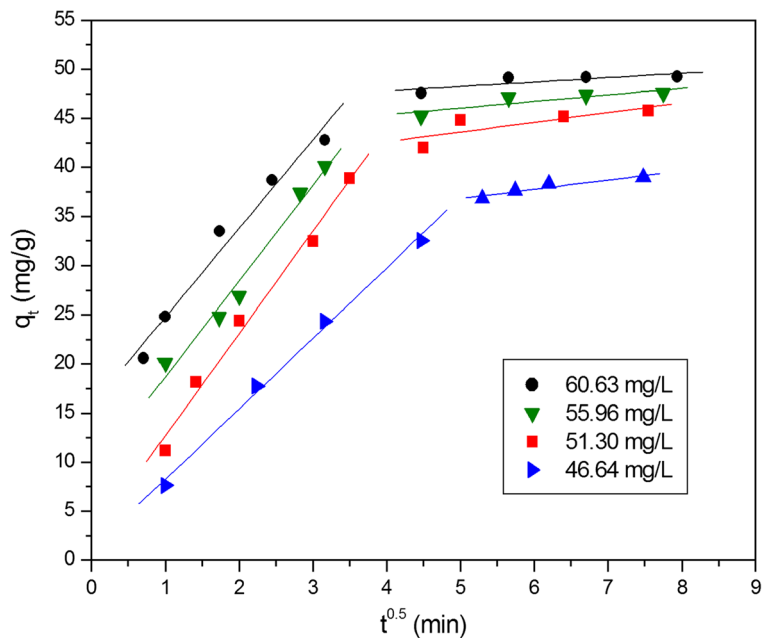
between ln (q_e/C_e) and $1/T$ as indicated by Eq. 6. In the meantime, the value of ΔG° was resolved from Eq. 7 (Table 3).

$$\ln\left(\frac{q_e}{C_e}\right) = \frac{\Delta S^\circ}{R} - \frac{\Delta H^\circ}{RT} \qquad (6)$$

$$\Delta G^\circ = \Delta H^\circ - T\Delta S^\circ \qquad (7)$$

where T (K) is the absolute temperature and R (8.314 J/mol/K) is the universal gas constant.

It would appear that the adsorption of IC onto AgNPs/f-silica is endothermic in nature due to the positive value of ΔH°. It has also been reported that the value of ΔH° gives valuable information about the adsorption type. For physical adsorption, the normal range of ΔH° is between 2.1 and 20.9 kJ/mol, and for chemical adsorption, it is between 20.9 and 418.4 kJ/mol (Karthik and Meenakshi 2015). In this study, the ΔH° value (14.95 kJ/mol) suggests that physical adsorption could be contributed to the removal of IC by the synthesized materials. The negative values of ΔG° reflected the spontaneous adsorption of dye on the adsorbent, and the positive values of ΔS° imply that the increased randomness at the solid–solution interface through the adsorption of IC from aqueous solution on AgNPs/f-silica. This is the normal outcome of the physisorption phenomenon, which takes place during electrostatic interactions (Ghaedi et al. 2012).

4.5 Adsorption Isotherms

Different isotherm models (Freundlich, Langmuir, Dubinin–Radushkevich (D–R), and Temkin) were used to recognize the nature of adsorption of IC on the synthesized materials. The suitability of the isotherm to describe the adsorption process was evaluated by the value of R^2 (correlation coefficient). The Langmuir

Table 3 Thermodynamic parameters for adsorption of IC dye (55.69 mg/L) on the AgNPs/f-silica sample (S1)

Temperature (°C)	ΔH° (kJ/mol)	ΔG° (kJ/mol)	ΔS° (J/mol/K)
25	14.95	− 16.45	103.65
30			
35			
40			

model adopts that the adsorption happens on a homogenous surface and no collaboration between adsorbates exists. The Langmuir isotherm was denoted by the following relation (Eq. 8):

$$\frac{C_e}{q_e} = \frac{C_e}{q_{max}} + \frac{1}{q_{max}K_L} \qquad (8)$$

where q_{max} (mg/g) denotes the maximum adsorption capacity of the synthesized adsorbents and K_L (L/mg) is the Langmuir constant. The Freundlich isotherm depicts the adsorption of the heterogeneous surface with adsorption sites that have diverse energies, and is represented by the following mathematical statement (Eq. 9):

$$\log q_e = \log K_F + \frac{1}{n}\log C_e \qquad (9)$$

where K_F (L/g) and n are the Freundlich constants and linked to the adsorption capacity and adsorption intensity, respectively. "With regard to Temkin model the adsorption heat of all the molecules in the layer supposed to be decreased with coverage owing to adsorbate–adsorbent interactions, and adsorption is characterized by a uniform distribution of binding energies, up to some maximum binding energy." The Temkin isotherm has been applied in the following form (Eq. 10) (Üner et al. 2016):

$$q_e = B\ln K_T + B\ln C_e \qquad (10)$$

where B denotes the heat of adsorption and is equal to (RT/b_T), where T is the absolute temperature, R is the gas constant (8.314 J/mol/K), b_T is the Temkin constant (J/mol), and K_T (L/g) is the equilibrium binding constant. The adsorption parameters for each model were determined and are given in Table 4. Screening of Table 4 reflects that the Langmuir isotherm model fits quite well with the experimental data (highest correlation coefficient values) than the Freundlich or Temkin model. The monolayer adsorption capacity (q_{max}) derived from this model was in the range of 64.26–73.05 mg/g at 30 °C. The fact that the Langmuir isotherm fits the experimental data very well might be a result of the homogeneous distribution of active sites onto the AgNPs/f-silica surface, since the Langmuir condition supposes that the surface is homogeneous.

Table 4 Langmuir, Freundlich, Dubinin–Radushkevich (D–R), and Temkin isotherm parameters and correlation coefficients for IC (55.69 mg/L) adsorbed onto the AgNPs/f-silica samples (0.01 g)

Model	Parameters	Synthesized composites		
		S3	S6	S12
Langmuir	K_L (L/mg)	0.0387	0.1511	0.1910
	q_{max} (mg/g)	64.26	69.50	73.05
	R_2	0.9889	0.9872	0.9997
Freundlich	K_F (L/g)	5.9265	10.309	16.058
	n	2.982	4.782	5.972
	R^2	0.8222	0.7869	0.9873
Temkin	B (J/mol)	9.755	8.351	7.035
	K_T	2.073	2.9136	3.342
	R_2	0.8333	0.7954	0.9782
D–R	q_s (mg/g)	33.01	37.11	41.03
	β (mol^2/kJ^2)	99.20	80.66	64.84
	E (kJ/mol)	0.071	0.079	0.087
	R^2	0.9620	0.9750	0.9910

Moreover, the adsorption intensity (n) of IC on the adsorbent revealed a value more than unity reflecting favorable adsorption conditions. In order to acquire more information about the mechanism of adsorption, the D–R isotherm was applied (Eq. 11).

$$\ln q_e = \ln q_s - \beta \varepsilon^2 \quad (11)$$

where q_S (mg/g) refers to the theoretical saturation capacity, β (mol^2/kJ^2) is the constant that gives information about the mean free energy of adsorption (E) per molecule of adsorbate, and ε is the Polanyi potential (J/mol) and can be determined from the following equation (Eq. 12):

$$\varepsilon = RT \ln\left(1 + \frac{1}{C_e}\right) \quad (12)$$

$$E = \frac{1}{\sqrt{2\beta}} \quad (13)$$

The adsorption mechanism can be clarified based on the value of the mean free energy (kJ/mol) (Eq. 13). The process follows physical adsorption if the value of E is < 8 kJ/mol. The value in the range of 8–16 kJ/mol indicates the occurrence of the chemical adsorption mechanism (Honfi et al. 2016;

Kara and Demirbel 2012). Herein, the values of E (Table 4) are 0.071, 0.079, and 0.087 kJ/mol (< 8 kJ/mol) for S3, S6, and S12, respectively, proposing a physisorption with a weak electrostatic attraction (Bouhamidi et al. 2017). The synthetic procedure for AgNPs/f-silica composites and also the possible mechanism for the adsorption of IC by the synthesized composites are represented in Scheme 1. The synthesis involves the reaction between silica silanol groups and APTMS to form amino-functionalized silica (f-silica). Then after the addition of silver ions in the presence of *Nigella sativa* extract, AgNPs are formed and attached to the surface (f-silica). The removal mechanism of the IC molecules by the synthesized materials can be proposed through weak electrostatic interactions (physical adsorption) between the silver moiety of the synthesized composites and the IC molecules, as had been reported in previous work (Dastafkan et al. 2015).

4.6 Comparison of AgNPs/f-Silica Adsorption Effectiveness with Other Adsorbents

A comparison of the maximum adsorption capability for IC on different adsorbents at room temperature is displayed in Table 5. It can be seen that the green synthesized composites (AgNPs/f-silica) illustrate enhanced adsorption capacity than the majority of the previously utilized adsorbents. Furthermore, the possibility of using the synthesized adsorbents more than one time was tested. After the dye adsorption process, the used adsorbent was washed well with ethanol and distilled water to remove the adsorbed dye and dried to use again for the next time. The adsorption–desorption processes were done for 6 cycles (Fig. 9). It was observed that the adsorption capacity of the selected composite (S6) slightly diminished with the increase of the reused cycle number and the removal efficiency of IC still maintained about 85.7% at the sixth cycle, which indicated that AgNPs/f-silica possessed superb stability. This might be ascribed to the strong AgNPs–support interaction reinforced by the rough surface of SiO$_2$, which contributed basically to anchoring nanoparticles and protected them from leaching (Guan et al. 2017). As a result, our materials (AgNPs/f-silica) are effective adsorbents to remove IC from aqueous solutions.

Table 5 Comparison of maximum adsorption capacities (q_{max}) of various adsorbents toward the removal of IC dye

Adsorbents	q_{max} (mg/g)	References
Coal fly ash	01.48	de Carvalho et al. (2011)
Zeolite from fly ash	01.23	de Carvalho et al. (2011)
Sawdust/$MnFe_2O_4$	01.74	Hashemian and Hidarian (2014)
Calcium hydroxide	00.95	Ramesh et al. (2015)
Montmorillonite	40.00	Geyikçi (2016)
Babool sawdust-activated carbon	38.31	Gupta and Lataye (2017)
Chitin nanowhisker-functionalized electrospun PVDF membrane	72.60	Gopi et al. (2017)
Mesoporous Mg/Fe double-layered hydroxide	62.80	Ahmed and Mohamed (2017)
AgNPs/f-silica	73.05	This work

5 Conclusion

In the current study, we demonstrated an eco-friendly, new, and simple method for AgNPs synthesis onto amino-functionalized silica using *Nigella sativa* aqueous extract as an efficient reducing agent. Immobilization of AgNPs on a surface would prevent its release into waterways, facilitating recovery of AgNPs and enabling them to be reused numerous times. The adsorption capacity of the synthesized samples (AgNPs/f-silica) was assessed by the adsorption of IC dye from aqueous solution.

The Langmuir model was more reasonable to depict the adsorption than the Freundlich one, and the maximum adsorption capacity of IC is 73.05 mg/g. The act of adsorption is reinforced via reactive sites present on the nanoscale surface compared to the diffusion of analyte into the pores of conventional sorbents. All thermodynamic parameters mentioned above indicate that the synthesized composites can be used as high-efficiency adsorbents to remove IC from aqueous solution. Immobilization of AgNPs on a surface may promote reuse, reduce the environmental risks associated with leaching of AgNPs, and enhance low cost.

Fig. 9 Removal percentage of IC after six adsorption/desorption cycles onto the AgNPs/f-silica sample (S6)
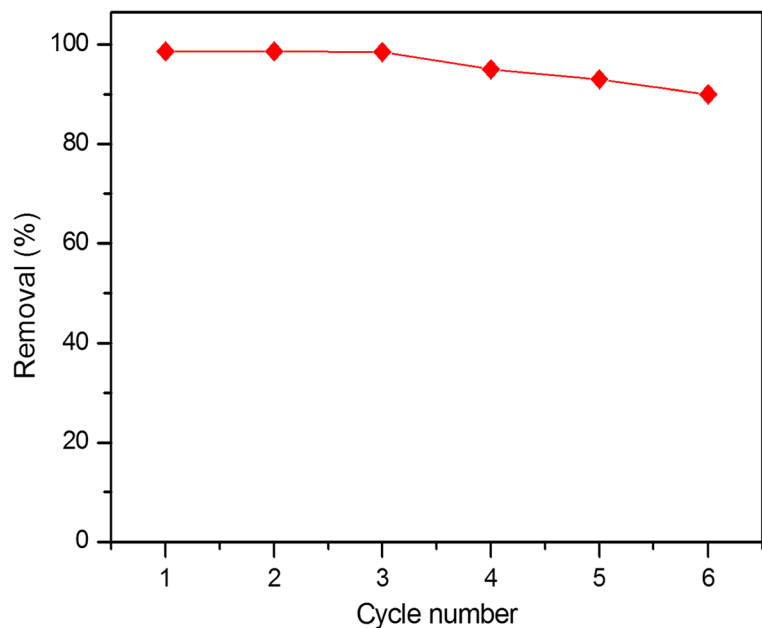
References

Aboelfetoh, E. F., & Pietschnig, R. (2009). Preparation and catalytic performance of Al2O3, TiO2 and SiO2 supported vanadium based-catalysts for C–H activation. *Catalysis Letters, 127,* 83–94.

Aboelfetoh, E. F., El-Shenody, R. A., & Ghobara, M. M. (2017). Eco-friendly synthesis of silver nanoparticles using green algae (Caulerpa serrulata): reaction optimization, catalytic and antibacterial activities. *Environmental Monitoring and Assessment, 189,* 349. https://doi.org/10.1007/s10661-017-6033-0.

Aboubaraka, A. E., Aboelfetoh, E. F., & Ebeid, E. Z. M. (2017). Coagulation effectiveness of graphene oxide for the removal of turbidity from raw surface water. *Chemosphere, 181,* 738–746.

Agnihotri, S., Mukherji, S., & Mukherji, S. (2014). Size-controlled silver nanoparticles synthesized over the range 5–100 nm using the same protocol and their antibacterial efficacy. *RSC Advances, 4,* 3974–3983.

Ahmed, M., & Mohamed, A. (2017). An efficient adsorption of indigo carmine dye from aqueous solution on mesoporous Mg/Fe layered double hydroxide nanoparticles prepared by controlled sol-gel route. *Chemosphere, 174,* 280–288.

Aljabre, S. H., Alakloby, O. M., & Randhawa, M. A. (2015). Dermatological effects of Nigella sativa. *Journal of Dermatology and Dermatologic Surgery, 19,* 92–98.

Amooaghaie, R., Saeri, M. R., & Azizi, M. (2015). Synthesis, characterization and biocompatibility of silver nanoparticles synthesized from Nigella sativa leaf extract in comparison with chemical silver nanoparticles. *Ecotoxicology and Environmental Safety, 120,* 400–408.

Ansari, R., & Mosayebzadeh, Z. (2011). Application of polyaniline as an efficient and novel adsorbent for azo dyes removal from textile wastewaters. *Chemical Papers, 65,* 1–8.

Banaei, A., Ebrahimi, S., Vojoudi, H., Karimi, S., Badiei, A., & Pourbasheer, E. (2017). Adsorption equilibrium and thermodynamics of anionic reactive dyes from aqueous solutions by using a new modified silica gel with 2,2′-(pentane-1,5-diylbis (oxy)) dibenzaldehyde. *Chemical Engineering Research and Design, 123,* 50–62.

Bhalara, P., Punetha, D., & Balasubramanian, K. (2015). Kinetic and isotherm analysis for selective thorium(IV) retrieval from aqueous environment using eco-friendly cellulose composite. *International Journal of Environmental Science and Technology, 12,* 3095–3106.

Bouhamidi, Y., Kaouah, F., Nouri, L., Boumaza, S., & Trari, M. (2017). Adsorption of diethyl and dibutyl phthalates onto activated carbon produced from Albizia julibrissin pods: kinetics and isotherms. *International Journal of Environmental Science and Technology, 14,* 271–284.

Dastafkan, K., Khajeh, M., Bohlooli, M., Ghaffari-Moghaddam, M., & Sheibani, N. (2015). Mechanism and behavior of silver nanoparticles in aqueous medium as adsorbent. *Talanta, 144,* 1377–1386.

de Carvalho, T. E., Fungaro, D. A., Magdalena, C. P., & Cunico, P. (2011). Adsorption of indigo carmine from aqueous solution using coal fly ash and zeolite from fly ash. *Journal of Radioanalytical and Nuclear Chemistry, 289,* 617–626.

Dhanalekshmi, K., & Meena, K. (2014). Comparison of antibacterial activities of Ag@TiO2 and Ag@SiO2 core–shell nanoparticles. *Spectrochimica Acta Part A: Molecular and Biomolecular Spectroscopy, 128,* 887–890.

Dolatyari, L., Yaftian, M. R., & Rostamnia, S. (2016). Removal of uranium(VI) ions from aqueous solutions using Schiff base functionalized SBA-15 mesoporous silica materials. *Journal of Environmental Management, 169,* 8–17.

Dong, Z., Le, X., Li, X., Zhang, W., Dong, C., & Ma, J. (2014). Silver nanoparticles immobilized on fibrous nano-silica as highly efficient and recyclable heterogeneous catalyst for reduction of 4-nitrophenol and 2-nitroaniline. *Applied Catalysis B: Environmental, 158,* 129–135.

Elmorsi, T. M. (2015). Synthesis of nano-titanium tannate as an adsorbent for crystal violet dye, kinetic and equilibrium isotherm studies. *Journal of Environmental Protection, 6,* 1454.

Elsupikhe, R. F., Shameli, K., & Ahmad, M. B. (2015). Sonochemical method for the synthesis of silver nanoparticles in κ-carrageenan from silver salt at different concentrations. *Research on Chemical Intermediates, 41,* 8515–8525.

Gabriel, J. S., Gonzaga, V. A., Poli, A. L., & Schmitt, C. C. (2017). Photochemical synthesis of silver nanoparticles on chitosans/montmorillonite nanocomposite films and antibacterial activity. *Carbohydrate Polymers, 171,* 202–210.

Gemeay, A. H., Elsharkawy, R. G., & Aboelfetoh, E. F. (2017). Graphene oxide/polyaniline/manganese oxide ternary nanocomposites, facile synthesis, characterization, and application for indigo carmine removal. *Journal of Polymers and the Environment,* 1–15. https://doi.org/10.1007/s10924-017-0947-z.

Geyikçi, F. (2016). Factorial design analysis for adsorption of Indigo Carmine onto Montmorillonite-Evaluation of the kinetics and equilibrium data. *Progress in Organic Coatings, 98,* 28–34.

Ghaedi, M., Sadeghian, B., Pebdani, A. A., Sahraei, R., Daneshfar, A., & Duran, C. (2012). Kinetics, thermodynamics and equilibrium evaluation of direct yellow 12 removal by adsorption onto silver nanoparticles loaded activated carbon. *Chemical Engineering Journal, 187,* 133–141.

Ghosh, S., & Vandana, V. (2017). Nano-structured mesoporous silica/silver composite: synthesis, characterization and targeted application towards water purification. *Materials Research Bulletin, 88,* 291–300.

Gopi, S., Balakrishnan, P., Pius, A., & Thomas, S. (2017). Chitin nanowhisker (ChNW)-functionalized electrospun PVDF membrane for enhanced removal of Indigo carmine. Carbohydrate Polymers, 165, 115–122.

Guan, H., Chao, C., Kong, W., Hu, Z., Zhao, Y., Yuan, S., & Zhang, B. (2017). Magnetic porous PtNi/SiO2 nanofibers for catalytic hydrogenation of p-nitrophenol. *Journal of Nanoparticle Research, 19,* 187.

Gupta, T. B., & Lataye, D. H. (2017). Adsorption of Indigo Carmine dye onto Acacia Nilotica (Babool) sawdust activated carbon. *Journal of Hazardous, Toxic, and Radioactive Waste, 21,* 1–11. https://doi.org/10.1061/(ASCE)HZ.2153-5515.0000365.

Habib, R., Asif, M. B., Iftekhar, S., Khan, Z., Gurung, K., Srivastava, V., & Sillanpää, M. (2017). Influence of relaxation modes on membrane fouling in submerged membrane

bioreactor for domestic wastewater treatment. *Chemosphere, 181*, 19–25.

Hashemian, S., & Hidarian, M. (2014). Synthesize and characterization of sawdust/MnFe2O4 nano composite for removal of indigo carmine from aqueous solutions. *Oriental Journal of Chemistry, 30*, 1753–1762.

Honfi, K., Tálos, K., Kőnig-Péter, A., Kilár, F., & Pernyeszi, T. (2016). Copper(II) and phenol adsorption by cell surface treated Candida tropicalis cells in aqueous suspension. *Water, Air, & Soil Pollution, 227*, 61.

Ider, M., Abderrafi, K., Eddahbi, A., Ouaskit, S., & Kassiba, A. (2017). Rapid synthesis of silver nanoparticles by microwave-polyol method with the assistance of latex copolymer. *Journal of Cluster Science, 28*, 1025–1040.

Jal, P., Patel, S., & Mishra, B. (2004). Chemical modification of silica surface by immobilization of functional groups for extractive concentration of metal ions. *Talanta, 62*, 1005–1028.

Kara, A., & Demirbel, E. (2012). Kinetic, isotherm and thermodynamic analysis on adsorption of Cr(VI) ions from aqueous solutions by synthesis and characterization of magnetic-poly (divinylbenzene-vinylimidazole) microbeads. *Water, Air, & Soil Pollution, 223*, 2387–2403.

Karthik, R., & Meenakshi, S. (2015). Removal of hexavalent chromium ions from aqueous solution using chitosan/polypyrrole composite. *Desalination and Water Treatment, 56*, 1587–1600.

Khdary, N. H., Ghanem, M. A., Merajuddine, M. G., & Manie, F. M. B. (2014). Incorporation of Cu, Fe, Ag, and Au nanoparticles in mercapto-silica (MOS) and their CO2 adsorption capacities. *Journal of CO2 Utilization, 5*, 17–23. https://doi.org/10.1016/j.jcou.2013.11.003.

Khurana, I., Saxena, A., Khurana, J. M., & Rai, P. K. (2017). Removal of dyes using graphene-based composites: a review. *Water, Air, & Soil Pollution, 228*, 180.

Liu, J.-f., Chao, J.-b., Liu, R., Tan, Z.-q., Yin, Y.-g., Wu, Y., & Jiang, G.-b. (2009). Cloud point extraction as an advantageous preconcentration approach for analysis of trace silver nanoparticles in environmental waters. *Analytical Chemistry, 81*, 6496–6502.

Mosbah, R., Djerrou, Z., & Mantovani, A. (2017). Protective effect of *Nigella sativa* oil against acetamiprid induced reproductive toxicity in male rats. *Drug and Chemical Toxicology*, 1–7. https://doi.org/10.1080/01480545.2017.1337127.

Nasretdinova, G. R., Fazleeva, R. R., Mukhitova, R. K., Nizameev, I. R., Kadirov, M. K., Ziganshina, A. Y., & Yanilkin, V. V. (2015). Electrochemical synthesis of silver nanoparticles in solution. *Electrochemistry Communications, 50*, 69–72.

Ncube, T., Kumar Reddy, K. S., Al Shoaibi, A., & Srinivasakannan, C. (2017). Benzene, toluene, m-xylene adsorption on silica-based adsorbents. *Energy and Fuels, 31*, 1882–1888.

Nivetha, K., & Prasanna, G. (2016). GC-MS and FT-IR analysis of Nigella sativa L. seeds. *Int J Adv Res Biol Sci, 3*, 45–54.

Ramesh, T. N., Kirana, D. V., Ashwini, A., & Manasa, T. (2015). Calcium hydroxide as low cost adsorbent for the effective removal of indigo carmine dye in water. *Journal of Saudi Chemical Society, 21*, 165–171.

Randhawa, M. A., Alenazy, A. K., Alrowaili, M. G., & Basha, J. (2017). An active principle of Nigella sativa L., thymoquinone, showing significant antimicrobial activity against anaerobic bacteria. *Journal of Intercultural Ethnopharmacology, 6*, 97.

Siddiqui, M. N., Redhwi, H. H., Achilias, D. S., Kosmidou, E., Vakalopoulou, E., & Ioannidou, M. D. (2017). Green synthesis of silver nanoparticles and study of their antimicrobial properties. *Journal of Polymers and the Environment*, 1–11. https://doi.org/10.1007/s10924-017-0962-0.

Sinha, T., Ahmaruzzaman, M., Bhattacharjee, A., Asif, M., & Gupta, V. (2015). Lithium dodecyl sulphate assisted synthesis of Ag nanoparticles and its exploitation as a catalyst for the removal of toxic dyes. *Journal of Molecular Liquids, 201*, 113–123.

Sun, Q., Cai, X., Li, J., Zheng, M., Chen, Z., & Yu, C.-P. (2014). Green synthesis of silver nanoparticles using tea leaf extract and evaluation of their stability and antibacterial activity. *Colloids and Surfaces A: Physicochemical and Engineering Aspects, 444*, 226–231.

Üner, O., Geçgel, Ü., & Bayrak, Y. (2016). Adsorption of methylene blue by an efficient activated carbon prepared from Citrullus lanatus. *Water, Air, & Soil Pollution, 227*, 1–15.

Venkatesham, M., Ayodhya, D., Madhusudhan, A., Kumari, A. S., Veerabhadram, G., & Mangatayaru, K. G. (2014). A novel green synthesis of silver nanoparticles using gum karaya: characterization, antimicrobial and catalytic activity studies. *Journal of Cluster Science, 25*, 409–422.

Vilchis-Nestor, A.-R., Trujillo-Reyes, J., Colín-Molina, J., Sánchez-Mendieta, V., & Avalos-Borja, M. (2014). Biogenic silver nanoparticles on carbonaceous material from sewage sludge for degradation of methylene blue in aqueous solution. *International Journal of Environmental Science and Technology, 11*, 977–986.

Wu, J., Wang, J., Du, Y., Li, H., & Jia, X. (2016). Adsorption mechanism and kinetics of azo dye chemicals on oxide nanotubes: a case study using porous CeO2. *Journal of Nanoparticle Research, 18*, 1–13.

Yoncheva, K., et al. (2014). Functionalized mesoporous silica nanoparticles for oral delivery of budesonide. *Journal of Solid State Chemistry, 211*, 154–161.

Yuan, S., Zhang, J., Yang, Z., Liang, B., & Tang, S. (2017). Click functionalization of poly(glycidyl methacrylate) microspheres with triazole-4-carboxylic acid for the effective adsorption of Pb(II) ions. *New Journal of Chemistry, 41*, 6475–6488.

Yue, Y., et al. (2017). γ-Irradiation assisted synthesis of graphene oxide sheets supported Ag nanoparticles with single crystalline structure and parabolic distribution from interlamellar limitation. *Applied Surface Science, 403*, 282–293.

Zhang, L., Liu, J., Yang, J., Yang, Q., & Li, C. (2008). Direct synthesis of highly ordered amine-functionalized mesoporous ethane-silicas. *Microporous and Mesoporous Materials, 109*, 172–183.

Zhang, Z.-h., Zhang, J.-l., Liu, J.-m., Xiong, Z.-h., & Chen, X. (2016). Selective and competitive adsorption of azo dyes on the metal–organic framework ZIF-67. *Water, Air, & Soil Pollution, 227*, 471.

Zhu, Q., Zhou, H.-l., Song, Y.-x., Chang, Z.-d., & Li, W.-j. (2017). Modification and investigation of silica particles as a foam stabilizer. *International Journal of Minerals, Metallurgy, and Materials, 24*, 208–215.